

## **Detection of enzyme activity in orthotopic murine breast cancer by fluorescence lifetime imaging using a fluorescence resonance energy transfer–based molecular probe**

Metasebya Solomon  
Kevin Guo  
Gail P. Sudlow  
Mikhail Y. Berezin  
W. Barry Edwards  
Samuel Achilefu  
Walter J. Akers

# Detection of enzyme activity in orthotopic murine breast cancer by fluorescence lifetime imaging using a fluorescence resonance energy transfer–based molecular probe

Metasebya Solomon,<sup>a,b</sup> Kevin Guo,<sup>a</sup> Gail P. Sudlow,<sup>a</sup> Mikhail Y. Berezin,<sup>a</sup> W. Barry Edwards,<sup>a</sup> Samuel Achilefu,<sup>a,b,c</sup> and Walter J. Akers<sup>a</sup>

<sup>a</sup>Washington University, Department of Radiology, Optical Radiology Laboratory, 4525 Scott Avenue, St. Louis, Missouri 63110

<sup>b</sup>Washington University, Department of Biomedical Engineering, 4525 Scott Avenue, St. Louis, Missouri 63110

<sup>c</sup>Washington University, Department of Biochemistry and Molecular Biophysics, 4525 Scott Avenue, St. Louis, Missouri 63110

**Abstract.** Cancer-related enzyme activity can be detected noninvasively using activatable fluorescent molecular probes. In contrast to “always-on” fluorescent molecular probes, activatable probes are relatively nonfluorescent at the time of administration due to intramolecular fluorescence resonance energy transfer (FRET). Enzyme-mediated hydrolysis of peptide linkers results in reduced FRET and increase of fluorescence yield. Separation of signal from active and inactive probe can be difficult with conventional intensity-based fluorescence imaging. Fluorescence lifetime (FLT) measurement is an alternative method to detect changes in FRET. Thus, we investigate FLT imaging for *in vivo* detection of FRET-based molecular probe activation in an orthotopic breast cancer model. Indeed, the measured FLT of the enzyme-activatable molecular probe increases from 0.62 ns just after injection to 0.78 ns in tumor tissue after 4 h. A significant increase in FLT is not observed for an always-on targeted molecular probe with the same fluorescent reporter. These results show that FLT contrast is a powerful addition to preclinical imaging because it can report molecular activity *in vivo* due to changes in FRET. Fluorescence lifetime imaging exploits unique characteristics of fluorescent molecular probes that can be further translated into clinical applications, including noninvasive detection of cancer-related enzyme activity. © 2011 Society of Photo-Optical Instrumentation Engineers (SPIE). [DOI: 10.1117/1.3594153]

Keywords: breast cancer; molecular imaging; time-domain; fluorescence energy transfer.

Paper 11105R received Mar. 7, 2011; revised manuscript received Apr. 22, 2011; accepted for publication May 4, 2011; published online Jun. 22, 2011.

## 1 Introduction

Molecular signatures of cancer tissues include upregulated signaling receptors and enzyme expression. For example, upregulation of integrin receptors in tumors is associated with metastatic spread.<sup>1</sup> Likewise, increased activity of members of the matrix metalloproteinase (MMPs) family in cancer tissue can also be an indication of metastatic potential.<sup>2</sup> Enzyme activity can be diagnostic and prognostic in cancer and other diseases. For instance, MMPs are biomarkers for diagnosis and prognosis in cancer as they have been implicated as mediators of tumor growth, invasion, and metastasis.<sup>3–6</sup> MMP inhibitors are under investigation as anticancer agents.<sup>2</sup>

Preclinical optical imaging with fluorescent contrast agents has become prominent in recent years due to the high sensitivity and high-throughput nature of this versatile modality. Fluorescent molecular probes can be administered for rapid detection of disease throughout the body of small animals, economically and without ionizing radiation. Use of fluorescent reporters that act in the near-infrared (NIR) are optimal for *in vivo* imaging due to

the higher penetration of this wavelength range relative to visible light.<sup>7,8</sup> Fluorescence techniques can be further enhanced by sensing mechanisms, such as spectral shifts, quenching, and fluorescence lifetime changes that may occur due to molecular interactions and environmental conditions. Optical imaging with fluorescent molecular probes is an economical, high-throughput modality for noninvasive detection these cancer signatures in animal models of cancer.

Fluorescent molecular probes include always-on agents that rely on target binding in tissues or activatable agents that report molecular interactions by signal enhancement mechanisms. For always-on agents, measured fluorescence intensity is used as a measure of concentration in tissue, similar to nuclear imaging. An example would be a ligand for an upregulated receptor that bears an NIR fluorescent reporter.<sup>8</sup> Activatable probes used in fluorescence-based imaging are optically invisible or at least display reduced fluorescence until molecular activation at the disease site. These include enzyme substrates with fluorescent dyes in close proximity that often employ fluorescence resonance energy transfer (FRET) in addition to other quenching

Address all correspondence to: Walter Akers, Washington University, Optical Radiology Laboratory, Department of Radiology, 4525 Scott Avenue, Campus Box 8225, St. Louis, Missouri 63110; Tel: 314-286-2015; Fax: 314-747-5191; E-mail: akersw@mir.wustl.edu.

mechanisms.<sup>6</sup> The enhancement of fluorescence intensity at the site of disease may be great enough in intensity for visualization but may not totally reflect molecular events within the disease site. Measurement of fluorescence lifetime alteration can be additionally utilized to verify that the observed fluorescence is indeed mediated by a molecular target and not from other processes.<sup>9</sup>

Fluorescence lifetime is an intrinsic property of fluorescent reporters that is not dependent on concentration but can reflect changes in the environment. Often, the quantum yield is directly related to the fluorescence lifetime: energy transfer between fluorescent reporters held in close proximity results in lower quantum yield as well as shortening of the fluorescence lifetime of the donor.<sup>10</sup> In the case of quenched molecular probes, the quantum yield and lifetime are subsequently restored to the free dye values after proteolysis, leading to an increase in fluorescence intensity and, we hypothesized, the lifetime values of the donor.

Briefly, the lifetime of an organic fluorophore is dependent on the rates of the radiative process (fluorescence,  $k_f$ ) and nonradiative processes  $k_{nr}$  (quenching) as stated in Eq. (1). Nonradiative processes include effects due to solvent interactions, temperature, and quenching,

$$\tau = \frac{1}{k_f + k_{nr}}. \quad (1)$$

Energy transfer from the excited-state molecule to an adjacent molecule, as in FRET, results in quenching of fluorescence and lower quantum yield. This increase in  $k_{nr}$  also results in shorter  $\tau$ . Detection of FRET between fluorescent protein pairs using fluorescence lifetime imaging microscopy is more accurate and precise than ratiometric methods.<sup>9</sup> Figure 1 shows a schematic of the mechanism of action of enzyme activatable probe, such as the one used in this study. The donor (D) is a NIR fluorescent reporter attached via a cleavable peptide linker to an acceptor (A) molecule. The absorption properties of the acceptor overlap with the emission properties of the donor attenuating fluorescence and

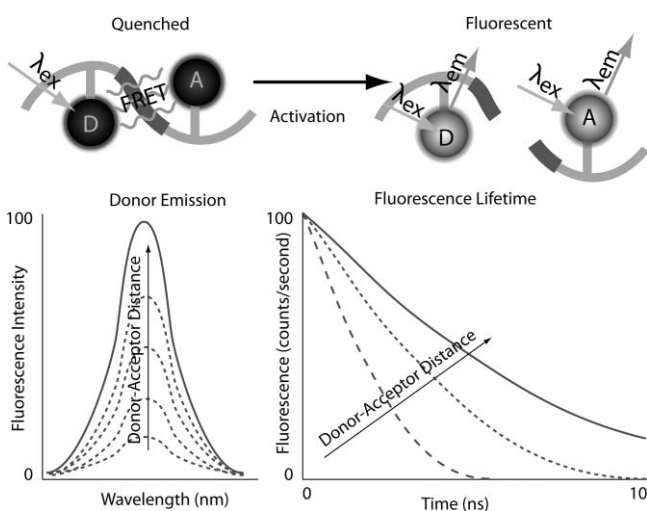


**Fig. 1** Cartoon of FRET-based fluorescent molecular probe and restoration of fluorescence after enzyme-mediated hydrolysis of the connecting peptide by protease enzymes. The fluorescence quantum yield and fluorescence lifetime of the donor are increased as the donor and acceptor are separated. In the case of MMP750, the donor and acceptor are identical fluorophores.

shortening lifetime of the donor. Upon enzyme-mediated hydrolysis, the emission properties of the donor are restored. This phenomenon is typically observed when the donor and acceptor are different fluorophores (heteroFRET) and may also occur with identical fluorophores (homoFRET).<sup>10–12</sup> Previously reported protease activatable molecular probes have shown to improve the tumor-detection sensitivity using the intensity signal.<sup>13,14</sup> In this paper, we demonstrate that fluorescence lifetime measurement confirms that the observed fluorescence in the syngeneic tumor is, in part, a result of MMP-mediated hydrolysis and subsequent liberation of the proteolytic fragments from close proximity that caused the initial quenching.

Herein, we examined an MMP-sensitive activatable fluorescent construct and an always-on heterodimeric  $\alpha v\beta 3$  integrin receptor (ABIR) targeted fluorescent probe in a murine orthotopic breast cancer model using both fluorescence intensity and fluorescence lifetime imaging. Although both agents produced good tumor contrast in this model, only the activatable probe showed a significant increase in fluorescence lifetime, validating the upregulated enzyme activity due to the presence of the tumor. This study demonstrates the potential of fluorescence lifetime imaging for improving the knowledge of whether the molecular events that are observed are actually target related with FRET-based activatable probes.

## 2 Methods

### 2.1 In Vitro Spectroscopy

IntegriSense 750 (IS750) and MMPsense 750 FAST (MMP750) were purchased from VisEn Medical (Bedford, Massachusetts) and prepared according to the manufacturer's instructions. IntegriSense750, MMP750, and MMP-activated MMP750 were diluted in 4% (w/v%) bovine serum albumin in phosphate-buffered saline for spectroscopy. A 20- $\mu$ L MMP750 solution was then added and incubated at 37°C for 3 h. Activation of MMP750 was confirmed by an increase in fluorescence intensity in cuvettes (ex/em: 740/755–900 nm) of the activated solution relative to the control solution under identical conditions. Fluorescence lifetime (FLT) measurements were performed with using 780 nm NanoLed<sup>®</sup> (impulse repetition rate, 1 MHz) excitation at 90 deg to the a time-correlated single-photon-counting detector at 820 nm, 26 nm bandpass (Horiba). The fluorescence intensity (yield) was recorded on a 50-ns scale until a peak of 5000 counts. The instrument response function was obtained using a Rayleigh scatter of Ludox-40 (0.05% in water) in an acrylic transparent cuvette at 780-nm emission. Decay analysis software (DAS6 v6.1; Horiba) was used for lifetime calculations. The goodness of fit was judged by  $\chi^2$  values, Durbin-Watson parameters, as well as visual observations of fitted line, residuals, and autocorrelation functions.

The overlap integral for FRET was calculated for the NIR fluorescent dye based on absorption and emission spectra using software developed in our lab. The FRET efficiency was calculated using the following approximations based on our experience of NIR fluorescent cyanine dyes: Quantum yield of donor: 0.1; molar absorptivity of acceptor:  $2 \times 10^5 \text{ M}^{-1} \text{ cm}^{-1}$ .

### 2.2 In Vivo imaging

All animal studies were performed according to protocols approved by at Washington University School of Medicine

Animal Studies Committee for humane care and use of laboratory animals. Luciferase-transfected 4T1 mouse mammary carcinoma cells (4T1*luc*, Sibtech, Brookfield, Connecticut) cultured in Dulbecco's Modified Eagle Medium (DMEM) media were injected subcutaneously into left and right mammary fat pads.

Mice were anesthetized with ketamine (85 mg/kg) and xylazine (15 mg/kg), intraperitoneal injection (IP) for depilation, intravenous injections, and initial postinjection imaging. For extended and subsequent imaging, isoflurane gas (2% v/v in 100% O<sub>2</sub>) was delivered via nosecone for maintenance of anesthesia. Imaging agents were administered according to manufacturer's recommendations, 1 nmol per mouse, via lateral tail vein of six- to eight-week-old female balb/c nude mice ( $n = 3$ ) provided by NCI (NIH).<sup>15</sup>

Time-domain diffuse optical imaging of living mice was performed using the eXplore Optix MX2 system (Advanced Research Technologies, Montreal, Canada) as reported previously.<sup>16</sup> Briefly, the animals were positioned supine on the heated imaging platform. Preinjection scans were performed to assess background and autofluorescence signals. Scans were again performed immediately post-injection and at 4–6 and 24 h postinjection. Regions of interest (ROI) including tumor and nontumor tissue were raster-scanned at 780-nm excitation with emission detection centered at 830 nm in 1.5-mm steps. Fluorescence intensity and lifetime values were determined by integration or single exponential fitting of the acquired temporal point-spread function (TPSF) fluorescence decay curves for each measurement using Optiview software (Advanced Research Technologies, Montreal, Canada). Images were created by mapping each value to the corresponding location on a white-light reference image of the mouse. Mean fluorescence intensity and lifetime values for tumor and nontumor tissue ROI for each mouse were selected and reported for analysis.

For reference and *ex vivo* fluorescence biodistribution assays, images were also captured using the Pearl NIR fluorescence imaging system (LiCor Biosciences, Lincoln, Nebraska). The biodistribution of probes was assessed using the simple method described previously.<sup>17,18</sup> At 24 h postinjection, aliquots of blood and pieces of major organs (tumor, heart, kidney, lung, spleen, stomach, intestine, muscle, liver, skin, and brain) were harvested and placed on a clear plastic Petri dish for imaging. Fluorescence images were acquired as previously described. Mean fluorescence intensity was determined for each tissue by ROI analysis and combined for each group for statistical analysis.

### 2.3 Statistical Analysis

Mean fluorescence intensity and FLT values of ROI for each group were compared using Student's *t*-test with  $\alpha = 0.05$  set for significance. Fluorescence biodistribution ROI data were averaged for each organ tissue for IS750 and MMP750, and plotted together for comparison.

## 3 Results

The partial *in vitro* activation of MMP750 by the enzyme led to the  $\sim 2\times$  increase in fluorescence as shown in Fig. 2(a). Such an increase in fluorescence was apparently due to the enzy-

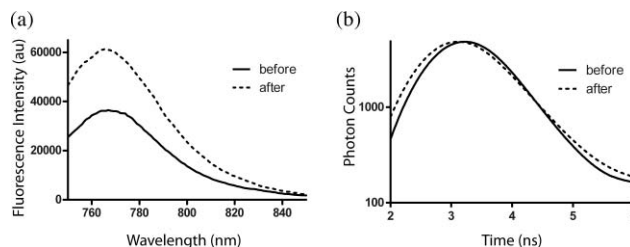


**Fig. 2** (a) Fluorescence steady-state spectra of MMP750 before and after enzymatic activation by MMP-2 for 3 h. The increase in fluorescence intensity confirmed partial activation by enzyme-mediated hydrolysis. (b) Fluorescence decays of MMP750 before and after MMP treatment demonstrating a shift in FLT from 0.58 to 0.73 ns due to decreased FRET efficiency after activation.

matic cleavage of the peptide linker, leading to the separation of the donor from the acceptor. As expected, a simultaneous increase of the decay slope [Fig. 2(b)] demonstrated an increase in the fluorescence lifetime from 0.58 to 0.73 ns, unequivocally demonstrating a reduction in FRET. The FRET efficiency was calculated to be 43.64%, which corresponds to the approximate doubling of fluorescence intensity after activation *in vitro* [Fig. 2(a)].

Having demonstrated the fluorescence lifetime increase in MMP750 on interaction with MMP and stable fluorescence lifetime of IS750, we administered the probes into small animal tumor models for *in vivo* imaging. Both IS750 and MMP750 showed tumor-specific uptake *in vivo* by fluorescence intensity imaging [Fig. 3(a)].

Fluorescence intensity values were highest for the ABIR-targeted probe immediately after injection in the tumor and nontumor regions and decreased with time. In contrast, MMP750 was relatively silent after injection and fluorescence signal increased with time, particularly in the tumor regions. *Ex vivo* tumor fluorescence at 24 h postinjection was higher in the tumor than other tissues [Fig. 3(b)], with 20-fold higher than muscle for both probes ( $n = 3$ ). Autofluorescence and signal from the GI tract was <10% of the signal after molecular probe administration and did not affect the measurement of fluorescence intensities or lifetimes.

Example fluorescence decay curves and nonlinear regression fits are given in Fig. 4. Laser power and integration time were automatically adjusted during scanning to ensure adequate photon counts for fitting. The tails of the TPSF curves were fit from 2 to 6 ns (Fig. 4, black lines) for image map construction.

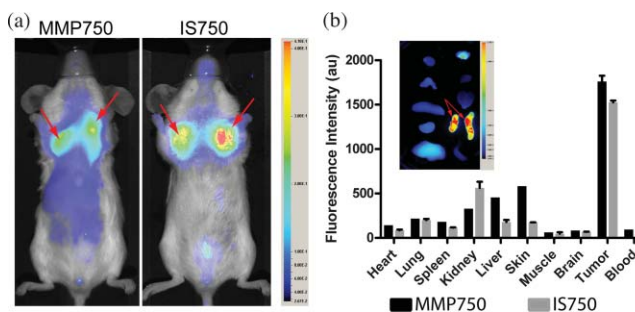


**Fig. 3** (a) Planar fluorescence imaging of mouse with orthotopic breast tumors at 4–6 h after injection of MMP750 or IS750. (b) Fluorescence biodistribution image (inset) and ROI data for organ tissues 24 h after injection of either MMP750 or IS750. Arrows indicate 4T1*luc* tumors.

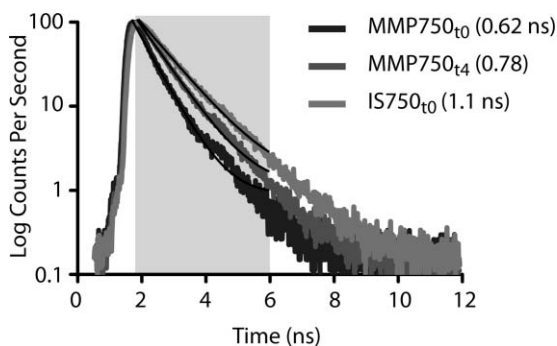


**Fig. 4** Representative normalized fluorescence decay curves (TPSF) *in vivo* FLT imaging tumor ROIs with single exponential least-squares nonlinear regression (black line) from 2 to 6 ns (shaded) for MMP750 post-injection (MMP750<sub>t0</sub>) and 4 h postinjection (MMP750<sub>t4</sub>). Fluorescence decay curves for IS750 were not significantly different between time points; thus, only one representative curve is shown.

Intensity maps created by integration of the fluorescence decay curves produced image maps showing good tumor contrast. The fluorescence intensity of MMP750 was very low immediately after injection and increased about 10-fold by 6 h postinjection [Figs. 5(a) and 5(b), respectively]. On the other hand, IS750 fluorescence was high immediately after injection [Fig. 5(e)]. The fluorescence signal from the tumor regions was significantly higher ( $P < 0.01$ ) for animals in both groups by 6 h postinjection [Figs. 5(b) and 5(f)].

*In vivo* FLT imaging showed that the measured tumor FLT's for MMP750 were longer at 4–6 h postinjection [Fig. 5(d)] relative to earlier time points [Fig. 5(c)]. The FLT maps showed a more diffuse pattern than the intensity maps with an increase in FLT in the tumor and peritumoral regions. For IS750, the

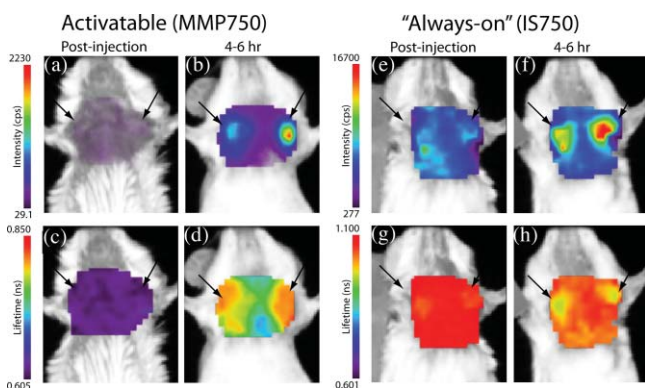


**Fig. 5** Fluorescence intensity and lifetime maps of mice with orthotopic 4T1 *luc* breast tumors immediately after (a,c) and 4–6 h after (b,d) injection of MMP750. The fluorescence intensity maps show low fluorescence (a) immediately after injection and (b) high signal from the tumors at 4–6 hr after injection (arrows). The fluorescence lifetime map is relatively flat with average FLT of 0.63 ns (c) immediately after injection. At 4–6 h after injection, the tumor areas show a higher FLT (0.76 ns) relative to nontumor regions. Corresponding image maps show different behavior for the always-on probe. The fluorescence intensity maps show higher signal (e) immediately after injection and from the tumors (f) at 4–6 hr after injection (arrows). The fluorescence lifetime map is relatively flat (g) immediately after injection. (h) At 4–6 h after injection, the tumor areas show a shorter FLT relative to nontumor regions.

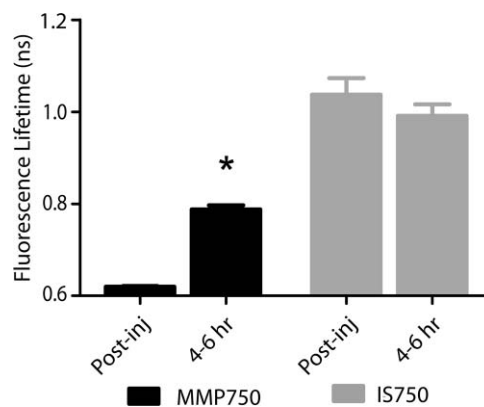


**Fig. 6** Graphical comparison of *in vivo* FLT values for tumor ROIs immediately after (postinjection) and at 4–6 hr after intravenous administration of NIR fluorescent molecular probes. The measured FLT values for MMP750 FAST at 4–6 h were significantly higher ( $*P < 0.01$ ) than postinjection. FLT values were not significantly different for these time points with IntegriSense750.

FLT maps were relatively flat at corresponding time points [Figs. 5(g) and 5(h)]. FLT values from *in vivo* ROI analysis are shown in Fig. 6.

For MMP750, the fluorescence lifetime was  $0.63 \pm 0.02$  ns immediately postinjection and increased with time. At 4–6 h postinjection, the FLT had increased significantly ( $P < 0.01$ ) to  $(0.76 \pm 0.02)$  ns in the tumor region. For IS750, the average FLT values did not change significantly ( $1.11 \pm 0.01$  ns immediately postinjection and  $1.10 \pm 0.03$  ns at 4–6 h postinjection). In the tumor regions, FLT values were slightly lower ( $1.09 \pm 0.03$  ns) than nontumor regions ( $1.11 \pm 0.03$  ns). Expression of MMP-2 and MMP-9 in the 4T1 *luc* tumor tissues was confirmed by immunohistochemistry (Fig. 7).

## 4 Discussion

Enzyme activatable fluorescent probes promise higher disease-specific contrast relative to “always-on” targeted molecular probes by fluorescence enhancement only within the tissue of interest. The contrast enhancement mechanism of fluorescence activation is unique to optical imaging. Detection of cancer-related enzyme activity using protease-activatable fluorescent probes has high potential for use in staging of primary cancers and detection of metastases.

In the current study, excellent tumor-specific contrast was achieved within 4–6 h postinjection with both the activatable MMP-sensitive and always-on integrin-targeted NIR fluorescent molecular probes in the orthotopic breast cancer model. The orthotopic breast tumors developed from implanted 4T1 cells syngeneic to the balb/c mouse line are known to produce metastases to the lungs and lymph nodes.<sup>19</sup> This aggressive tumor model is representative of fast-growing and invasive human breast cancer. MMP activity and ABIR expression are biomarkers of breast cancer considered to indicate the aggressiveness of the disease.<sup>20,21</sup>

The molecular targets, MMPs and ABIR, are ubiquitously expressed in both target and nontarget tissues, although at unequal levels.<sup>1,2</sup> Thus, it is not surprising that some fluorescence signal is observed in nontarget tissues. Enhancement of signal from the

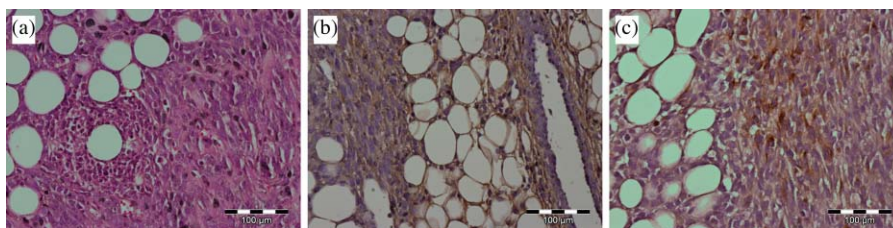


**Fig. 7** H&E-stained section of (a) orthotopic 4T1Luc tumor tissue and immunohistochemistry for (b)MMP-2, and (c) MMP-9. Darker staining indicates areas with high MMP expression in these tumors.

MMP probe was observed in these tissues and results in some fluorescent background rendering the tumor-to-normal contrast produced by this agent almost equal to that of the always-on fluorescent probe. It is therefore imperative that the activation of this probe be established to distinguish enzyme activity from other modes of contrast including nonspecific accumulation. The activation of MMP750 and resulting change in FLT appears to have occurred from reduction in FRET as the peptide sequence was cleaved as depicted in Fig. 1, although other mechanisms may also be involved. FLT imaging provides confirmatory evidence of activation by detecting changes in FRET.

Unsurprisingly, the FLT increase due to activation of MMP750 is seen in the tumor tissue and the surrounding mammary tissue as well [Fig. 5(d)]. High MMP activity in the tumor periphery is expected as MMPs are expressed within the tumor stroma and on the invasive front.<sup>2</sup> Thus, the FLT map demonstrates the real MMP activity in tissue rather than just accumulation. This study shows that detection of molecular probe activation using FLT-based imaging has significant advantages over other strategies, such as inclusion of a spectrally distinct, reference fluorescent reporter either co-injected<sup>22</sup> or as part of the probe construct.<sup>14</sup> The use of a single fluorophore as both donor and acceptor facilitates synthesis of activatable probes, providing that adequate quenching is established.

A shortcoming of enzyme-activatable probes, which is not often discussed, is whether there is significant tumoral accumulation of fluorescent proteolytic fragments that were activated distal to the tumor site. Accumulation of the proteolytic fragments might exaggerate the apparent enzyme activity within the tumor tissue. Further studies are needed to assess this type of nonspecific activation and the fates of the probe fragments within the body. Fluorescent probes with improved enzyme selectivity will improve detection and differentiation of cancer-related enzyme activity from other causes, such as inflammation.<sup>23</sup> MMP750 resulted in exceptional tumor-specific contrast by fluorescence intensity that was apparently enzyme mediated. Good tumor-normal contrast was obtained within 4–6 h after injection, a significant improvement over larger, polymeric activatable probes that require 8–24 h.<sup>22</sup>

## 5 Conclusion

For quantitative measurement of enzyme activity, nonspecific activation must be minimized or other methods developed to separate the level of activation from that of concentration. We have presented FLT imaging as one possibility. FLT imaging has the potential for directly assessing changes in FRET due to enzyme activity and is relatively simple and inexpensive relative

to other methods, such as reference probe coadministration and multimodal imaging. Measurement of the change in FRET on activation was performed using a single excitation/emission and simple data analysis. FLT imaging using NIR fluorescent FRET probes is a promising technique that has translational potential in regions accessible to optical imaging such as skin, gastrointestinal, and breast cancers. This technique may also be useful for fluorescence guidance of surgery.

## Acknowledgments

This research was supported in part by Grants No. K01RR026095 (Akers) from the National Center for Research Resources, No. R01 EB008111 (Achilefu), No. R21 CA131660–02 (Edwards), and No. R21 CA149814–01 (Berezin). Mice and imaging agents were purchased as part of the National Cancer Institute Cancer Imaging Workshop.<sup>15</sup> The content is solely the responsibility of the authors and does not necessarily represent the official views of the National Center for Research Resources, National Institute of Biomedical Imaging and Bioengineering, and National Cancer Institute of the National Institutes of Health.

## References

1. E. K. Sloan, N. Pouliot, K. L. Stanley, J. Chia, J. M. Moseley, D. K. Hards, and R. L. Anderson, "Tumor-specific expression of alphavbeta3 integrin promotes spontaneous metastasis of breast cancer to bone," *Breast Cancer Res.* **8**(2), R20 (2006).
2. R. Roy, J. Yang, and M. A. Moses, "Matrix metalloproteinases as novel biomarkers and potential therapeutic targets in human cancer," *J. Clin. Oncol.* **27**(31), 5287–5297 (2009).
3. C. Bremer, S. Bredow, U. Mahmood, R. Weissleder, and C. H. Tung, "Optical imaging of matrix metalloproteinase-2 activity in tumors: feasibility study in a mouse model," *Radiology* **221**(2), 523–529 (2001).
4. B. P. Himelstein, R. Canete-Soler, E. J. Bernhard, D. W. Dilks, and R. J. Muschel, "Metalloproteinases in tumor progression: the contribution of MMP-9," *Invasion & Metastasis.* **14**(1–6), 246–258.
5. B. Fingleton, Matrix metalloproteinase inhibitors for cancer therapy: the current situation and future prospects. *Expert Opinion on Therapeutic Targets* **7**(3), 385–397 (2003).
6. R. Weissleder, C. H. Tung, U. Mahmood, and A. Bogdanov, Jr., "In vivo imaging of tumors with protease-activated near-infrared fluorescent probes," *Nat. Biotechnol.* **17**(4), 375–378 (1999).
7. V. Ntziachristos, J. Ripoll, L. V. Wang, and R. Weissleder, "Looking and listening to light: the evolution of whole-body photonic imaging," *Nat. Biotechnol.* **23**(3), 313–320 (2005).
8. S. Achilefu, "Lighting up tumors with receptor-specific optical molecular probes," *Technol. Cancer Res. Treat.* **3**(4), 393–409 (2004).
9. C. W. Chang, M. Wu, S. D. Merajver, and M. A. Mycek, "Physiological fluorescence lifetime imaging microscopy improves Forster resonance

- energy transfer detection in living cells," *J. Biomed. Opt.* **14**(6), 060502 (2009).
10. M. Y. Berezin, and S. Achilefu, "Fluorescence lifetime measurements and biological imaging," *Chem. Rev.* **110**(5), 2641–2684.
  11. J. A. Levitt, D. R. Matthews, S. M. Ameer-Beg, and K. Suhling, "Fluorescence lifetime and polarization-resolved imaging in cell biology," *Curr. Opin. Biotechnol.* **20**(1), 28–36 (2009).
  12. S. V. Koushik and S. S. Vogel, "Energy migration alters the fluorescence lifetime of Cerulean: implications for fluorescence lifetime imaging Forster resonance energy transfer measurements," *J. Biomed. Opt.* **13**(3), 031204 (2008).
  13. U. Mahmood and R. Weissleder, "Near-infrared optical imaging of proteases in cancer," *Molecular Cancer Therapeutics* **2**(5), 489–496 (2003).
  14. R. L. Scherer, J. O. McIntyre, and L. M. Matrisian, "Imaging matrix metalloproteinases in cancer," *Cancer Metastasis Rev.* **27**(4), 679–690 (2008).
  15. "NCI Imaging Camp."
  16. S. Achilefu, S. Bloch, M. A. Markiewicz, T. Zhong, Y. Ye, R. B. Dorshow, B. Chance, and K. Liang, "Synergistic effects of light-emitting probes and peptides for targeting and monitoring integrin expression," *Proc. Natl. Acad. Sci. U S A* **102**(22), 7976–7981 (2005).
  17. S. Achilefu, R. B. Dorshow, J. E. Bugaj, and R. Rajagopalan, "Novel receptor-targeted fluorescent contrast agents for in vivo tumor imaging," *Invest. Radiol.* **35**(8), 479–485 (2000).
  18. J. E. Bugaj, S. Achilefu, R. B. Dorshow, and R. Rajagopalan, "Novel fluorescent contrast agents for optical imaging of in vivo tumors based on a receptor-targeted dye-peptide conjugate platform," *J. Biomed. Opt.* **6**(2), 122–133 (2001).
  19. K. Tao, M. Fang, J. Alroy, and G. G. Sahagian, "Imagable 4T1 model for the study of late stage breast cancer," *BMC Cancer* **8**, 228 (2008).
  20. A. Daniele, A. F. Zito, G. Giannelli, R. Divella, M. Asselti, A. Mazzocca, A. Paradiso, and M. Qua, "Expression of metalloproteinases MMP-2 and MMP-9 in sentinel lymph node and serum of patients with metastatic and non-metastatic breast cancer," *Anticancer Res.* **30**(9), 3521–3527.
  21. P. M. McGowan and M. J. Duffy, "Matrix metalloproteinase expression and outcome in patients with breast cancer: analysis of a published database," *Ann. Oncol.* **19**(9), 1566–1572 (2008).
  22. J. Baeten, J. Haller, H. Shih, and V. Ntziachristos, "In vivo investigation of breast cancer progression by use of an internal control," *Neoplasia* **11**(3), 220–227 (2009).
  23. C. Bremer, C. H. Tung, and R. Weissleder, "In vivo molecular target assessment of matrix metalloproteinase inhibition," *Nat. Med.* **7**(6), 743–748 (2001).